Bioorganic Chemistry 92 (2019) 103078

Contents lists available at ScienceDirect

Bioorganic Chemistry

journal homepage: www.elsevier.com/locate/bioorg

Molecular interaction of manganese based carbon monoxide releasing molecule (MnCORM) with human serum albumin (HSA)

Pitchavel Vidhyapriya[a], Dhanaraj Divya[b], Bala. Manimaran[b], Natarajan Sakthivel[a,*]

[a] Department of Biotechnology, Pondicherry University, Puducherry 605 014, India
[b] Department of Chemistry, Pondicherry University, Puducherry 605 014, India

ARTICLE INFO

Keywords:
Carbon monoxide releasing molecule
Human serum albumin
Fluorescence
Mixed quenching
Prodrug

ABSTRACT

In the present study, the interaction between the HSA and MnCORM *in vitro* under physiological conditions, was investigated through ultraviolet-visible (UV-vis) absorption, fluorescence, time-resolved fluorescence, circular dichroism (CD), Fourier transform infrared (FT-IR) spectroscopic techniques and *in silico* molecular docking methods. Binding parameters such as the binding constant, number of binding sites and binding force were obtained from the fluorescence data. Thermodynamic interaction revealed that the reaction was spontaneous ($\Delta G < 0$) and hydrogen bond and van der Waals interaction were primarily involved in the binding. The changes induced in the secondary structure conformation due to the MnCORM interaction were monitored using CD and FT-IR spectroscopic techniques. The results showed reduction in α-helix conformation and corresponding increase in β-sheet and unordered structures due to slight unfolding. The time-resolved fluorescence decay confirmed the static quenching mechanism of the MnCORM. The molecular docking studies revealed that the MnCORM interacted at Sudlow's site II of domain IIIA through hydrogen bond and van der Waals interactions. In order to understand the drug distribution and elimination, studies on the drug molecule interaction with HSA are vital. Therefore, it is evident that MnCORM interacts with HSA through ground state complex formation and thus suitable for *in vivo* delivery.

1. Introduction

Albumin is the major constituent of serum proteins. It is employed in delivery of various exogenous and endogenous substances, drugs and pharmaceuticals due to its binding efficiency. Serum albumin is considered as a model protein for studying drug-protein interaction *in vitro*. It has the ability to bind insoluble substances and various drug molecules are dependent on the binding capacity toward serum albumins which is an important parameter in pharmacokinetics. Human serum albumin (HSA) accounts for approximately 60% of the total amount of protein, corresponding to a concentration of 40 mg/ml in blood and provides about 80% of the osmotic pressure of blood [1]. HSA protects bound drugs against oxidation and regulates *in vivo* distribution. Considering the advantages of HSA, it is important to study the drug HSA interactions when developing new drugs [2]. HSA is a globular protein composed of structurally similar α-helical domains (I,II,III) and subdomains (A and B) (Fig. 1). Overall, there are seven binding sites in the HSA. The two main binding sites known as Sudlow's sites I and II are located in the IIA and IIIA subdomains and the latter has higher solvent accessibility. The other five binding sites have high affinity for fatty acids. Moreover, HSA binds to heme and porphyrins making it suitable for photodynamic therapy [3,4]. Sudlow's site I is basically dominated by strong hydrophobic interaction whereas site II is dominated by van der Waals, dipole-dipole and hydrogen-bonding interactions with aromatic carboxylic acids [5]. There are numerous drugs such as lidocaine interacting with IB domain, warfarin with IIA domain, ibuprofen interacting with IIIA and IIIB domains and also, metals such as Au^{+}, Pt^{+} bind at IA and Zn^{2+}, Ni^{2+}, Cd^{2+} etc. bind at multi-metal binding IIA domains and propofol at binding site of IIIB domain [6]. HSA contains 1 tryptophan, 18 tyrosine and 31 phenylalanine residues and therefore the intrinsic fluorescence of these aromatic amino acid residues can be studied using fluorescence spectroscopy to characterize the substrate to ligand binding effects [7]. The type of interactions may be due to the ionic association of amphiphilic molecules with proteins and enzymes, non-covalent association of proteins with fatty acids and other compounds containing non-polar groups and existence of hydrophobic

Abbreviations: CORM, carbon monoxide releasing molecule; HSA, human serum albumin; CD, circular dichroism; FT-IR, Fourier transform infrared spectroscopy; PBS, phosphate buffered saline; PDB, protein data bank; TCPSC, time-correlated single photon counting

* Corresponding author at: Department of Biotechnology, School of Life Sciences, Pondicherry University, Puducherry 605 014, India.
E-mail address: puns2005@gmail.com (N. Sakthivel).

https://doi.org/10.1016/j.bioorg.2019.103078
Received 19 January 2019; Received in revised form 12 June 2019; Accepted 17 June 2019
Available online 17 June 2019
0045-2068/

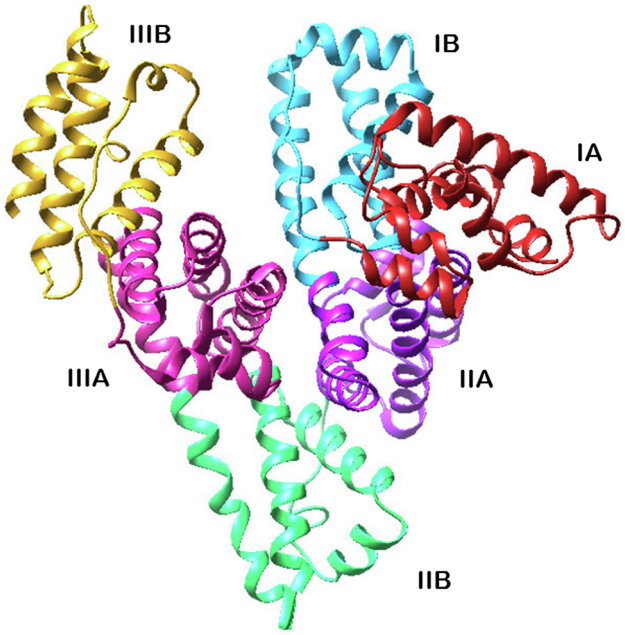

Fig. 1. Structure of human serum albumin showing subdomains, IA, IB, IIA, IIB, IIIA and IIIB.

interactions between non-polar residues of proteins with hydrophobic moieties of molecules [8]. The spectral changes observed on the binding of fluorophores with proteins are important tools for the investigation of the binding sites and conformational changes.

Carbon monoxide releasing molecules (CORMs) are capable of releasing CO spontaneously or in response to trigger. There are a few CORMs reported for their anti-microbial, anti-inflammatory, anti-proliferative and other biological functions. The controlled and localized delivery of CO at the target site is essential for therapeutics. The cellular uptake and specific delivery of CORMs in sufficient amount must be achieved *in vivo* for its activity. It is known that interaction between drug and protein is important in determining the biological activity of the CORM. Albumins are effective in increasing the solubility of hydrophobic drugs in plasma and thereby, facilitate their delivery to cell *in vivo* and *in vitro* [9]. There are reports about molybdenum based carbonyl complexes such as ALF414 [10] interacts with bovine serum albumin at domain IA (tryptophan 134) and ALF186 [11] interacts with HSA. The interaction of flavonol-based photoCORM with serum albumins at site I of domain IIA was also reported [12]. The HSA bound Cu (L)(PRD) [13] exhibited stronger anticancer activity and showed an enhanced target ability compared to the ligand alone. Similarly, the platinum(IV) based prodrug was reported for anticancer activity and also, in situ targeting to HSA proteins in blood [14].

Recently, we have reported an MnCORM (Fig. 2) which induces apoptosis through intrinsic pathway in cancer cells such as lung (A549), cervical (HeLa), colon (HCT-15) and breast (MDA MB-231) and suitable for photodynamic therapy [15]. Therefore, it is significant to evaluate the bioinorganic property of the MnCORM. In the present study, we have examined the molecular interaction of MnCORM with HSA using ultraviolet (UV), fluorescence, circular dichroism and FT-IR studies under physiological conditions and *in silico* docking studies. The complexation behavior of MnCORM was elucidated using UV-visible spectroscopic studies [16]. Fluorescence techniques were employed to determine the mechanism of quenching, quenching rate constant, binding constant, number of binding sites, thermodynamic parameters and nature of binding forces. The conformational changes in the protein were monitored using FT-IR spectroscopic studies and the ellipticity of the protein was measured using CD in the far UV regions [17]. The findings of the present investigation can be used for albumin-based drug delivery system.

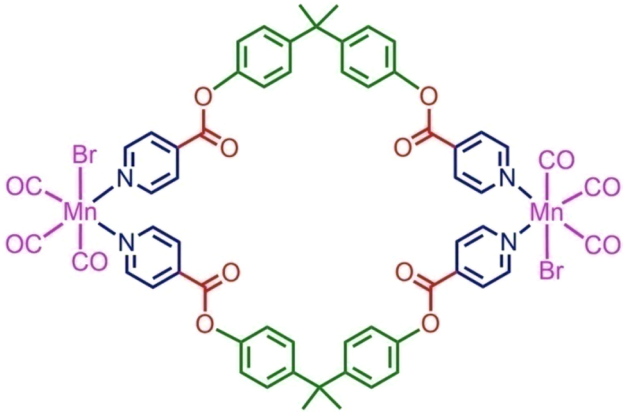

Fig. 2. Structure of MnCORM, M_2L_2-type dinuclear metallacyclophane $[Mn(CO)_3Br(\mu\text{-bpcpd})]_2$ [18].

2. Materials and methods

2.1. Chemicals

Human serum albumin (Himedia), 1 mM stock solution was freshly prepared in phosphate buffered saline (PBS), pH 7.4 and stored in dark at 4 °C. MnCORM was synthesized and 1 mM stock concentration of MnCORM was prepared in DMSO and stored in dark at 4 °C. Working concentrations were prepared by appropriate dilutions in PBS (pH 7.4).

2.2. Synthesis of MnCORM

The manganese based CORM (MnCORM), M_2L_2-type dinuclear metallacyclophane $[Mn(CO)_3Br(\mu\text{-bpcpd})]_2$ was synthesized using semi-rigid ester functionalized pyridyl ligand with organic spacer and metal precursor containing *fac*-$Mn(CO)_3$ core [18].

2.3. UV-visible absorption spectroscopy

UV-visible absorption measurement is a simple method that is used to investigate structural changes and to explore complex formation [19]. The experiment was performed with HSA and MnCORM in the ratio of 1:1 and absorbance was recorded in the range of λ 200 to 400 nm using Nanodrop. The UV spectra were recorded for 10 μM of HSA in PBS solution (physiological pH). The UV spectra were recorded for 10 μM of MnCORM. The absorption spectra were analyzed for any changes and complex formation [20].

2.4. Fluorescence spectroscopy

Fluorescence spectra were recorded at an excitation wavelength of λ 280 nm and the emission wavelength in the range of λ 300 to 450 nm using a SpectraMax multimode reader using a 96-well black plate. Both excitation and emission slit widths were set to 5 nm. HSA was prepared in PBS (pH 7.4) to give a final concentration of 30 μM and was maintained constant. The MnCORM was added to give a range of concentrations from 10 μM to 100 μM. The fluorescence emission was recorded three times and further analyzed for the type of interaction. Suitable buffer solutions were used as references when measuring the fluorescence spectra of protein solutions along with MnCORM [8].

2.5. Inner filter effect

In steady-state fluorescence experiments, the absorption spectrum of MnCORM overlapped with the excitation and emission wavelength of

HSA. Thus, it is very important to subtract an inner filter effect from the raw quenching data. Therefore, the fluorescence data was corrected for inner filter effect as per the following equation [21,22]:

$$F_{corr} = F_{obs} \times e^{(Aex+Aem)/2} \quad (1)$$

where F_{corr} and F_{obs} are the corrected and measured fluorescence intensity, respectively, A_{ex} and A_{em} are the absorbance at excitation (λ 280 nm) and emission wavelengths (λ 335 nm) of the sample respectively.

2.6. Measurement of circular dichroism (CD) spectra

The changes in the secondary structure of HSA were recorded in the range of λ 190–250 nm using an automatic recording spectropolarimeter (JASCO J-815) controlled by the Jasco software, with a 10 mm quartz cell in nitrogen atmosphere. HSA CD measurements in the presence and absence of MnCORM were performed with a scan rate of 100 nm/min. A stock solution of 1 μM HSA was prepared in PBS. The HSA concentration was held constant and the MnCORM concentration was varied as 0.5 and 1 μM in PBS. The buffer solution was chosen as the blank and was manually subtracted from each spectrum during scanning. Each sample was scanned three times and averaged for a CD spectrum.

2.7. Time resolved fluorescence (TRF)

Time-resolved fluorescence decay of HSA alone and in presence of different concentrations of MnCORM were measured by time-correlated single photon counting (TCPSC) methods using a Fluorolog-FL3-11 (Horiba Jobin Yvon) spectrofluorometer. Samples were excited at λ 280 nm using Xenon lamp source and the decay measurements were recorded at λ 335 nm. All measurements were performed in quartz cell of 1 cm path length. The lifetime components including decay time and relative amplitudes were calculated using decay analysis software and the goodness of fit was estimated based on reduced chi-square value (χ^2). The average fluorescence lifetime (τ_f) of triexponential iterative fitting was calculated from normalized pre-exponential factors and decay times using the equation:

$$\tau_f = \frac{\Sigma \alpha_i \tau^2}{\Sigma \alpha_i \tau} \quad (2)$$

2.8. FT-IR spectroscopy

FT-IR measurements were carried out at room temperature using a Nicolet iS5 FTIR spectrometer equipped with a germanium attenuated total reflection (ATR) accessory. All spectra were taken via 60 scans with a resolution of 0.4 cm^{-1}. The FT-IR spectra of HSA in the absence and presence of MnCORM were first collected in the range of ν 500 cm^{-1} and 4000 cm^{-1} and the absorbance of the buffer solution (PBS at pH 7.4) was then subtracted. The secondary structure content of the amide I region (ν 1600–1700 cm^{-1}) was deconvoluted by second derivative using MagicPlot.

2.9. Molecular docking of MnCORM and HSA

Molecular docking was performed using Autodock 4.2. Crystal structure of HSA was downloaded from RCSB protein data bank (PDB accession 1AO6) [20]. The MnCORM structure was drawn using Marvin sketch and saved in .mol2 format. The mode of interactions involved in the binding of MnCORM to HSA were predicted. All the crystallographic water molecules were removed from protein. The HSA was prepared for docking where polar hydrogens were added and Kollman charges were employed. The MnCORM structure was prepared by implementing Gasteiger charges and torsional angle set to zero. The protein and ligand were transformed into pdbqt format that contains atom coordinates, partial charges and also solvation parameters. Grid maps were calculated using Autogrid program. The docking was performed using Lamarckian genetic algorithm (GA). The Lamarckian GA was implemented for a maximum of 2.5×10^6 energy evaluations, selection, crossover and mutation rate of 0.02. The generated conformers were scored by energy-based AutoDock scoring function that includes scoring for hydrogen bonding, van der Waals and electrostatic interactions, loss of entropy due to ligand binding and solvation. The conformation with lowest binding energy and maximum number of hydrogen bonds was chosen for further analysis.

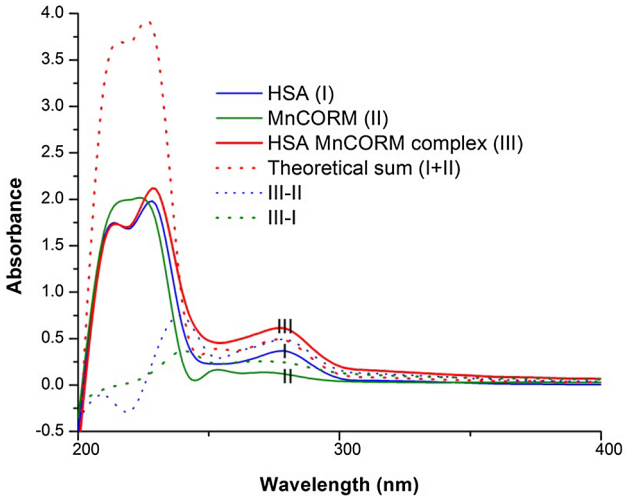

Fig. 3. UV absorption spectra in range of λ 200–400 nm. The solid lines represent the UV spectra of the HSA (blue), MnCORM (green) and the HSA MnCORM complex (1:1) (red). The dotted lines represent the theoretical absorbance of each spectra which is clearly different from solid lines denoting the interaction between HSA and MnCORM.

3. Results and disucssion

3.1. UV-visible absorption spectra

The result demonstrated the existence of an interaction between MnCORM and HSA (Fig. 3). HSA exhibited strong absorption peak at around λ 230 nm and weak absorption peak at around λ 280 nm which resulted from the aromatic amino acids (Trp, Tyr, and Phe). The strong absorption peak is typical of the backbone structure (α-helix) of HSA [19]. The change in absorbance at λ 230 nm reflects the perturbations in the secondary structure of protein. The absorption spectrum of the complex (III) was different from the summation of spectra of free HSA (I) and MnCORM (II) which confirms the ground state complex formation [23]. The increase in absorption at λ 280 nm indicates that the microenvironment around the aromatic residues was altered due to complexation [24]. There was no shift in the absorption peak at λ 280 nm. However, the increase in the absorption peak at λ 280 nm was due to the interaction of HSA with MnCORM which has to be further confirmed.

3.2. Fluorescence spectroscopy

3.2.1. Fluorescence emission spectra

The fluorescence intensities of free HSA and in the presence of various concentrations of MnCORM (10–100 μM) were recorded from λ 300 to 450 nm using an excitation filter of λ 280 nm (Fig. 4). There was a remarkable quenching observed with increasing concentrations of MnCORM [25]. Further the changes in the microenvironment, secondary structure of the protein and the mechanism of quenching and nature of interactions were evaluated.

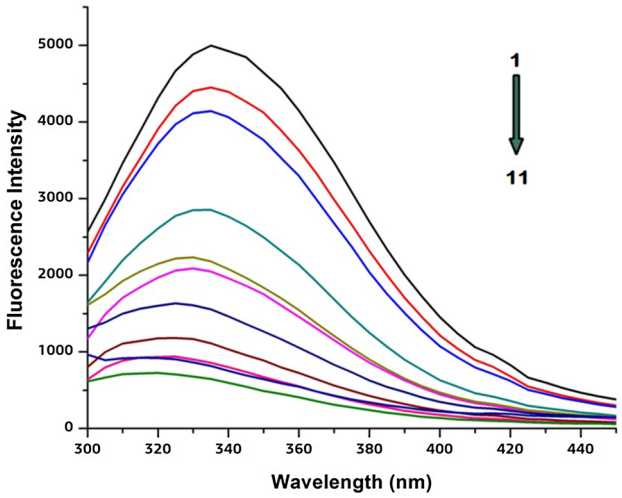

Fig. 4. The fluorescence spectra of HSA (30 μM) was recorded with increasing concentrations of MnCORM. The arrow 1–11 indicates the increasing concentration of MnCORM from 0 μM to 100 μM in order of 10 μM. λ_{ex} = 280 nm.

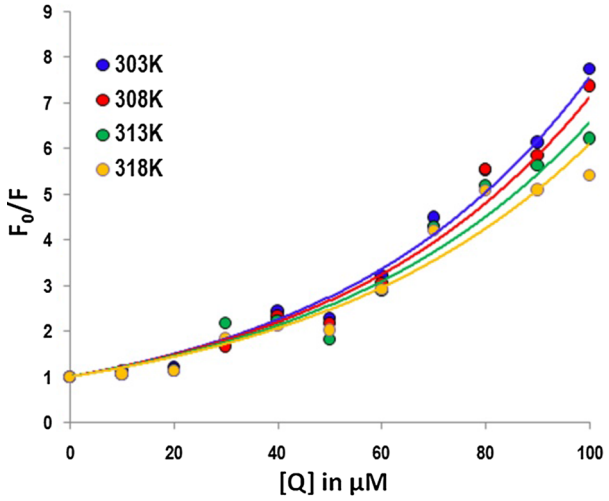

Fig. 5. The Stern-Volmer plots of F_o/F vs. [Q] at the four different temperatures.

3.2.2. Quenching mechanism analysis

Fluorescent quenching could be classified into static and dynamic based on its temperature and viscosity. The decrease in fluorescence in presence of quencher may be due to formation of ground state complex (static) or collision between molecules (dynamic). The quenching mechanism is classified as static, dynamic or mixed quenching and can be determined using Stern-Volmer constant (K_{SV}). In general, the plot of F_o/F vs [Q] yields a straight line and decrease in K_{SV} with an increase in temperature denotes static quenching and an increase in K_{SV} with an increase in temperature denotes dynamic quenching. The experimental data was recorded using suitable buffer solutions as blank and subtracted to avoid background of the fluorescence. The ability of MnCORM to absorb emitted light will increase due to spectral overlap. Therefore, the raw fluorescence was corrected for its inner filter effect [26].

(a) Stern Volmer equation

The HSA fluorescence quenching in the presence of various ligands is characterized by a line Stern-Volmer (SV) plot and is usually analyzed using the classical Stern-Volmer (SV) equation:

$$\frac{F_o}{F} = 1 + K_{SV}[Q] \quad (3)$$

where F_o and F are the steady state fluorescence intensities at the maximum wavelength in the absence and presence of quencher, respectively, [Q] is the quencher concentration and K_{SV} is the Stern-Volmer constant.

The plot of F_o/F vs [Q] yields an exponential curve (Fig. 5). An upward curvature of the Stern-Volmer plots has also been previously reported [27]. The data was rationalized by considering only the linear domain of the Stern-Volmer plot. The Stern Volmer quenching rate constant K_{SV} is a direct measure of the quenching efficiency. On the basis of K_{SV} determined from the Eq. (3), the MnCORM HSA complex was formed and resulted in adequate quenching [28]. The K_{SV} values decreased from 5.27 ± 0.31 to 4.15 ± 0.18 × 10^4. This result suggests that the quenching was due to static mechanism (Table 1). The decrease in the constant with respect to temperature indicates static quenching rather than collisional dynamic quenching. The decrease in the value of K_{SV} with respect to increasing temperature implies formation of a less stable HSA MnCORM complex at higher temperatures. Considering the dependence of binding constant on temperature, it is evident that a thermodynamic process was involved in the formation of a complex.

Table 1
Stern-Volmer and bimolecular quenching constant of HSA MnCORM complex at different temperatures.

Temperature, K	K_{SV} (×10^4 M^{-1})	K_q (×10^{13} $M^{-1}.s^{-1}$)	V (×10^4 M^{-1})
303	5.27 ± 0.31	5.27 ± 0.31	2.16 ± 0.30
308	5.01 ± 0.59	5.01 ± 0.59	2.15 ± 0.25
313	4.53 ± 0.29	4.53 ± 0.29	1.99 ± 0.56
318	4.15 ± 0.18	4.15 ± 0.18	1.92 ± 0.27

Further, considering the exponential form, the model of sphere of action another method of modified form of Stern-Volmer equation was used,

$$\frac{F_o}{F} = (1 + K_{SV}[Q]) \times e^{V[Q]} \quad (4)$$

where, F_o and F are the steady state fluorescence intensities at the maximum wavelength in the absence and presence of MnCORM, respectively, [Q] is the MnCORM concentration, K_{SV} is the Stern-Volmer constant and V is static quenching constant [29]. Instantaneous static quenching occurs when a quencher resides within the sphere of action (Table 1).

The appearance of upward curvature might be due to dynamic quenching or adequate quenching at higher concentrations [30]. The slope of the plot at lower concentrations of MnCORM was below 1 and it changes to greater than 1 at a ratio of 0.6 (HSA/MnCORM) suggesting mixed quenching. Therefore, it is necessary to determine the mode of quenching. Diffusion coefficients are larger at higher temperatures and therefore, the bimolecular quenching constants increase with respect to temperature for dynamic quenching.

$$K_{SV} = k_q \tau_0 \quad (5)$$

k_q is the bimolecular quenching rate constant, and τ_o is the average lifetime of the biomolecule in the absence of the quencher ($\tau_o = 10^{-9}$ s^{-1}) [31]. The K_{SV} was of the order of 10^4 and the k_q were of the order of 10^{13}. The rate constant for quenching due to diffusion of biopolymers 2 × 10^{10} M^{-1} s^{-1}. The values of k_q range from 4 × 10^{13} to 5 × 10^{13} and is larger than the acceptable limit of diffusional rate constant which further supported the static quenching mechanism (Table 1). Therefore, the upward curvature was due to adequate quenching and not due to dynamic quenching [32].

(b) Evaluation of the binding constant and the number of binding sites

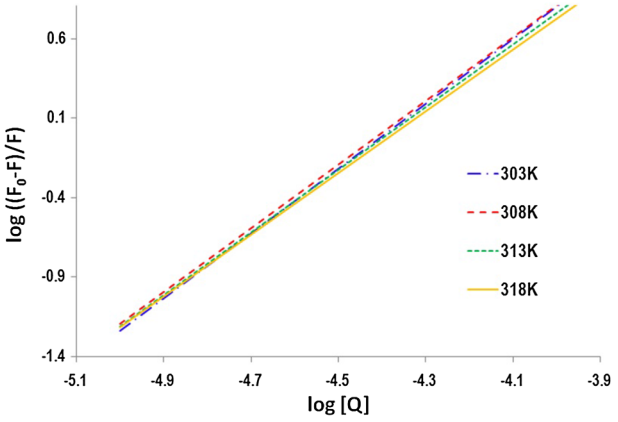

Fig. 6. Logarithmic plot of (F_o-F)/F vs [Q] at different temperatures.

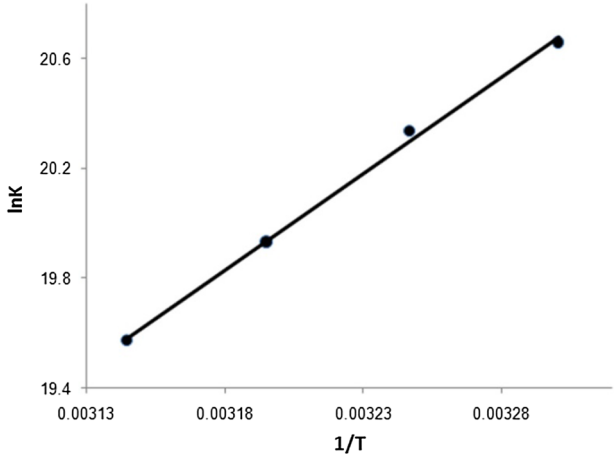

Fig. 7. Van't Hoff plot of lnK vs 1/T for HSA MnCORM complex.

For static quenching, the number of binding sites and the binding constant at different temperatures were determined by the equation [33]:

$$\log\frac{F_o - F}{F} = \log K_b + n\log[Q] \quad (6)$$

where F_o and F are the fluorescence intensities without and with the quencher [13]. The linear plot gives the slope value as n, the number of binding sites and the intercept values as log K_b (Fig. 6).

The binding constant, K_b is used to determine the affinity of ligand to protein (Table 2). The higher order of K_b suggests the specific binding affinity of ligand towards the protein HSA [33]. The reduction in binding constant (9.376 ± 1.68 to 3.170 ± 1.21 (10^7 M^{-1})) was in accordance with reduction in K_{SV} and k_q in Table 1 [34]. The decrease in K_b with respect to temperature was similar to the decrease in K_{SV} and confirm the static quenching process. Thus, it implies the formation of unstable complex during the binding process of HSA and MnCORM. The number of binding sites, n were approximately 2, indicating that there are two sites in the HSA protein for MnCORM to interact (Table 2). It is expected that when one binding site is occupied, the bound MnCORM may impose slight conformational changes in protein secondary structure, which may enhance interactions between protein-MnCORM complex at other site [28,35].

The binding constant values are significant in understanding the distribution of the drug in plasma. Weak binding of drug can lead to a short life time or poor distribution, while strong binding can decrease the concentration of free drug in plasma [36]. The reduction in the binding constant values (9.376 ± 1.68 to 3.170 ± 1.21 (10^7 M^{-1})) with an increase in temperature indicate the destabilization of the complex (Table 2). Further, these values reveal that MnCORM has good binding affinity for HSA and suitable for transport. The formation of a less stable complex ensures the distribution of MnCORM to the target sites [26,37].

(c) Thermodynamic parameters and nature of binding forces

The nature of binding forces that may be existent between a ligand and biomolecule are generally hydrogen bonds, van der Waals force, electrostatic and hydrophobic interactions. The signs of the enthalpy and entropy are important in determining the nature of the binding force. A positive value for both enthalpy change (ΔH^0) and entropy change (ΔS^0) indicate that the interactions are hydrophobic. A negative value for both ΔH^0 and ΔS^0 indicate that the interactions might be due to formation of multiple hydrogen bonds and van der Waals forces. When ΔH^0 is negative and ΔS^0 is positive, the interactions are electrostatic [38]. The change in Gibbs free energy with respect to temperature was calculated using Van't Hoff equation:

$$\ln K_b = -\frac{\Delta H^0}{RT} + \frac{\Delta S^0}{R} \quad (7)$$

where K_b is the binding constant at a given temperature and R is the gas constant.

The plot of lnK_b vs 1/T gave a straight line with the slope value corresponding to enthalpy change and the intercept value corresponding to entropy change (Fig. 7).

The calculated values of ΔH^0 and ΔS^0 were –5.86 × 10^4 J/mol K and –21.22 J/mol K respectively. Therefore, the interactions between HSA and MnCORM were due to hydrogen bonds and van der Waals forces [34]. The free energy change was calculated from the equation and tabulated:

$$\Delta G^0 = \Delta H^0 - T\Delta S^0 \quad (8)$$

The Gibbs free energy change decreased with increasing temperature and the negative signs for free energy (ΔG^0) of the HSA MnCORM complex indicate that the interaction is spontaneous (Table 3).

3.3. Measurement of CD spectra

The changes in the secondary structure of HSA in the presence of MnCORM were observed by monitoring the far UV spectra (Fig. 8). The tertiary and secondary structure changes of protein upon drug binding are important in determining ongoing changes. The characteristic α-helix of HSA is denoted by two minima at λ 208 and 222 nm [39–41].

Table 2
The binding constant and the number of binding sites at different temperatures for the HSA MnCORM system.

Temperature T(K)	Binding constant, Kb (×10^7) (M^{-1})	Number of binding sites, n
303	9.376 ± 1.68	2.042 ± 0.007
308	6.776 ± 1.43	2.005 ± 0.003
313	4.529 ± 1.09	1.973 ± 0.002
318	3.170 ± 1.21	1.943 ± 0.005

Table 3
Thermodynamic parameters at different temperatures for the HSA MnCORM complex.

Temperature T(K)	Free binding energy, ΔG^0 (×10^4) (J/mol K)	Enthalpy change, ΔH^0 (J/mol K)	Entropy change, ΔS^0 (J/mol K)
303	–5.21	−5.86 × 10^4	−21.22
308	–5.20		
313	–5.19		
318	–5.18		

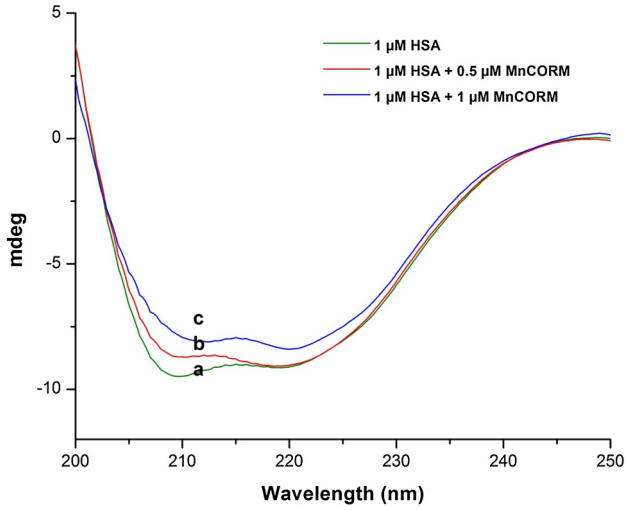

Fig. 8. Far UV CD spectra of HSA (1 μM) in the range of λ 200–250 nm (a) in absence of MnCORM (b) in presence of 0.5 μM MnCORM and (c) 1 μM MnCORM.

The ellipticity at λ 208 nm of HSA was monitored for secondary structural changes. The intensity of the negative peaks at λ 208 and 222 nm decrease in the presence of MnCORM. This change in the α-helical protein structure was observed due to the interaction of HSA with MnCORM. The helical content of HSA decreased from 69.3% to 46.7% due to interaction with MnCORM. There was increase in the β-sheet content from 4.5% to 10.6%, turn from 12.4% to 18.3% and unordered structures from 13.8% to 24.4%. The conformational change of HSA due to MnCORM binding was confirmed (Table 4).

The decrease in helicity of HSA on addition of MnCORM indicates that the MnCORM is bound to the amino acid residues of HSA. An increase in unordered coil and β-sheet structures were observed in HSA. The MnCORM can bind to HSA to form complexes and therefore, the interactions resulted in slight unfolding of the polypeptide backbone of native protein and further exposure of buried hydrophobic cavities [28,42]. Further, a blue shift in the emission maximum of HSA indicates a decrease in polarity of the surrounding microenvironment [1,43] (Fig. 4). It is proven from the similar shape that the helical secondary structure was predominantly retained although there was a decrease in the helical content (Fig. 8).

3.4. Time resolved fluorescence

The local changes in the structure of HSA due to the interaction of MnCORM was studied using Time-resolved fluorescence spectroscopy (Fig. 9). The fluorescent decay profile was used to study the interaction and changes due to the complex microenvironment. The average lifetime measurements were calculated for free HSA and with increasing concentrations of MnCORM. The triexponential decay function within acceptable χ^2 limits was used to determine the individual lifetime components [44,45]. The average lifetime of unquenched and quenched HSA remained almost the same and therefore the type of quenching mechanism was static (Table 5).

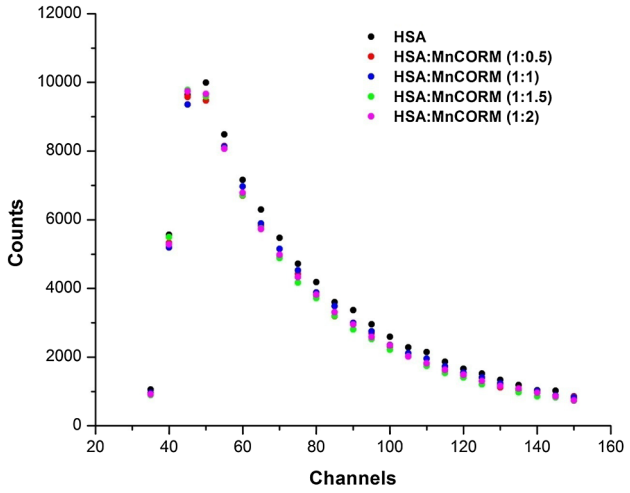

Fig. 9. Time-resolved fluorescence spectra of unquenched and quenched HSA with increasing concentrations of MnCORM. C_{HSA} = 10 μM and C_{MnCORM} = 5 μM to 20 μM in order of 5 μM.

Table 5
Fluorescence lifetime of free HSA and HSA with various concentrations of MnCORM.

HSA: MnCORM	τ_1 (ns)	τ_2 (ns)	τ_3 (ns)	α_1	α_2	α_3	t_f	χ^2
0	2.42	4.77	9.68	0.363	0.179	0.458	7.97	1.12
1:0.5	2.36	4.73	9.46	0.328	0.177	0.495	7.96	1.14
1:1	2.33	4.65	9.31	0.373	0.106	0.52	7.96	1.03
1:1.5	2.34	4.68	9.37	0.413	0.156	0.432	7.59	1.06
1:2	2.26	4.5	9.06	0.33	0.087	0.584	7.99	1.14

3.5. FT-IR spectroscopy

The FT-IR spectra were recorded at room temperature using Nicolet iS5 spectrometer. The spectra were recorded for 10 μM of free HSA, HSA:MnCORM (1:1) with PBS as blank (Fig. 10). The spectrum was deconvoluted and the curves were fitted by second order derivative. Amide I is the major band of the protein infrared spectrum and are associated with secondary structure conformations of the proteins. The FTIR of HSA showed that the absorbance corresponding to α-helix (ν 1653 cm^{-1}), β-sheet (ν 1622 and 1685 cm^{-1}), turns (ν 1662 and 1674 cm^{-1}) and random coil (ν 1642 cm^{-1}) regions shifted on interaction with MnCORM [46,47]. The secondary structure transitions were determined by the ratio of β-sheet/α-helix (ν 1685 cm^{-1}/1653 cm^{-1}) [48]. The value was 0.58 for the free HSA and increased to 1.19 for the HSA-MnCORM interaction confirming the increase in beta sheet conformation of HSA. The secondary structure content of free HSA alone was comprised of α-helix 52.82%, β-sheet 27.3%, turns 13.95% and random coils 3.68%. In the presence of MnCORM, the α-helix decreased to 45.17%, random coils to 2.14%, turns to 13.81% and β-sheet increased to 38.88%.

3.6. Molecular docking of MnCORM and HSA

Molecular docking was performed to understand the interactions between MnCORM and HSA. The best of the conformations was chosen

Table 4
Secondary structure content of free HSA and HSA MnCORM complex.

Concentration	Helix (%)	Beta sheet (%)	Turn (%)	Unordered (%)
1 μM HSA	69.3	4.5	12.4	13.8
1 μM HSA + 0.5 μM MnCORM	53.6	6.4	20.4	19.6
1 μm HSA + 1 μM MnCORM	46.7	10.6	18.3	24.4

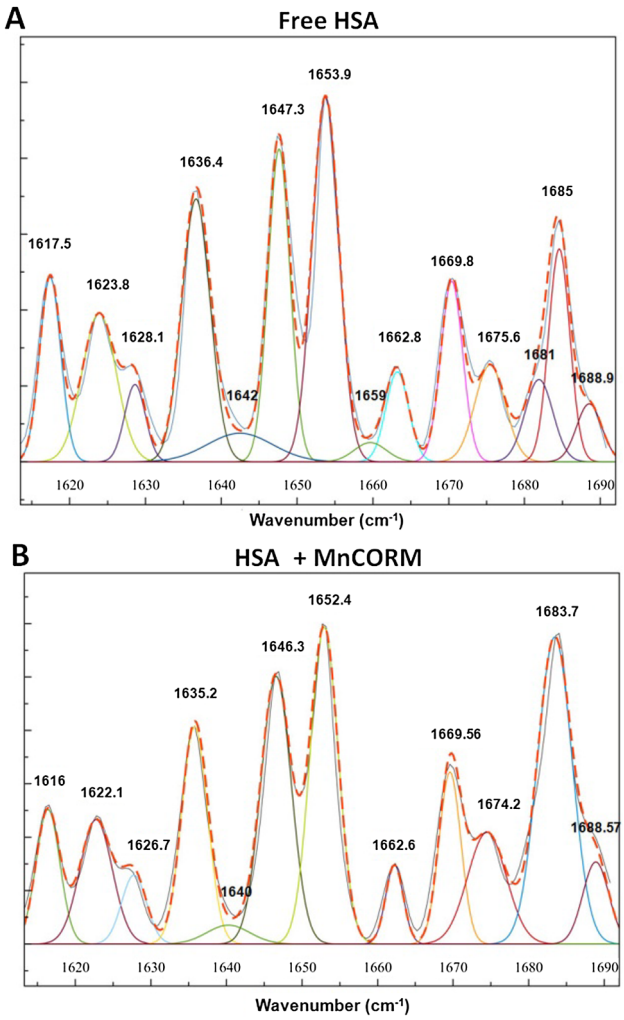

Fig. 10. FTIR spectra of amide I region (ν 1600–1700 cm^{-1}) of (a) free HSA (b) HSA:MnCORM (1:1). The dotted lines show the sum of all the fitted curves.

and the lowest binding energy was –9.59 kcal/mol (Fig. 11). The MnCORM binds with HSA at the Sudlow's site II (domain IIIA; residues 384–497). The site consists of several positively charged and hydrophobic residues in the pocket which enable the binding of MnCORM.

Table 6
Binding energy and interactions involved in HSA-MnCORM binding using Autodock 4.2.

Energy (kcal/mol)	Hydrogen bond atom from HSA	Hydrogen bond atom from MnCORM	Bond distance (Å)	Other interactions
–9.59	LYS439:HZ3 TYR401:HN LYS402:HN HIS440:HD1 HIS440:HA PRO441:HD1 GLU396:OE1	:UNK0:O11 :UNK0:O2 :UNK0:O2 :UNK0:O6 :UNK0:O6 :UNK0:O6 :UNK0:H13	2.0 3.0 2.6 2.6 2.2 2.3 2.5	Hydrophobic – Proline 441, π-alkyl interactions, Electrostatic – GLU 396, GLU 400, LYS 444

The MnCORM interacts with the HSA through polar groups and also hydrophobic interactions (Table 6). The MnCORM formed H-Bond interactions with positively charged amino acids such as Lys439, Tyr401, Lys402, His440 with a bond length of 2.0, 3.0, 2.6 Å respectively. The MnCORM formed two hydrogen bonds with negatively charged amino acid Glu396 with a bond length of 2.6 and 2.2 Å. Also, the ligand MnCORM interacted with non-polar amino acid Pro441 forming two hydrogen bonds with bond length of 2.7 and 2.5 Å. The Br atom of MnCORM also exhibited electrostatic interactions with Lys444. Apart from these, the MnCORM ligand had electrostatic interactions with Glu396 and Glu400. Hydrophobic interactions were also observed with Pro441 through its alkyl groups.

4. Conclusion

Molecular interaction of MnCORM with HSA under physiological conditions was investigated using UV-vis, fluorescence, FT-IR, circular dichroism and also *in silico* molecular docking. The UV-vis absorption studies suggested that the interaction between HSA and MnCORM was due to steady state complex formation. Further, based on the fluorescence studies, it was confirmed that the fluorescence quenching mechanism was static and there were 2 binding sites in the protein for interaction with MnCORM. The nature of interactions were predominantly due to hydrogen bonds and van der Waals and also, from the molecular docking studies, it was found that some electrostatic and hydrophobic interactions were involved in the binding of MnCORM to HSA. The changes in the secondary structure of HSA were revealed from the CD and FT-IR spectroscopic studies. Thus, present study, for the first time, confirmed the spontaneous interaction of anticancer molecule,

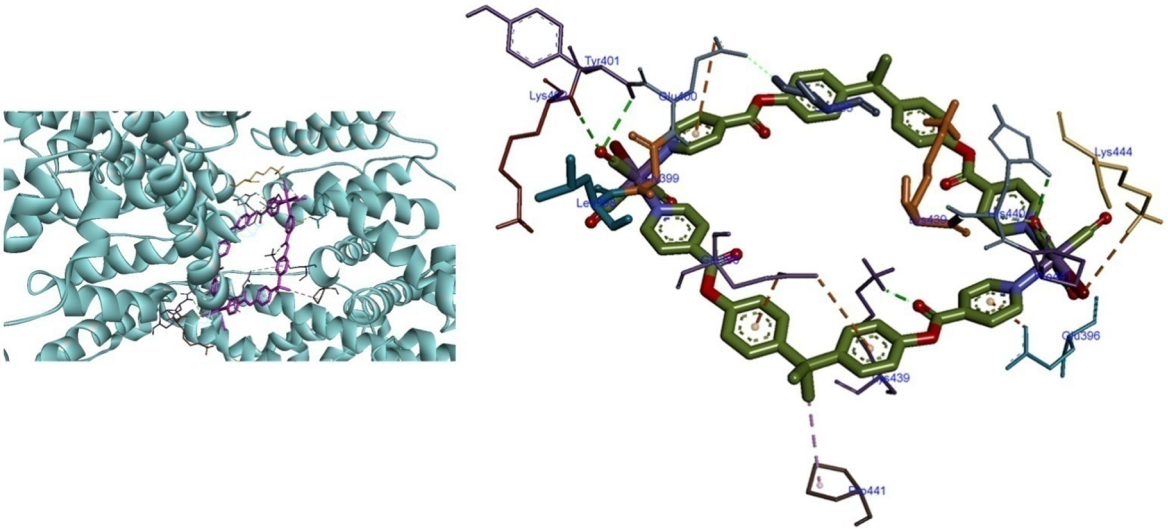

Fig. 11. Molecular docking of MnCORM and HSA. The interacting residues from HSA and atoms from MnCORM involved in the binding are depicted in the right.

MnCORM with HSA and the insight may facilitate further studies for albumin-based intracellular drug delivery system.

Declaration of Competing Interest

The authors declare that there are no conflicts of interest.

Acknowledgements

We thank DBT for providing Senior Research Fellowship to P. Vidhyapriya. The authors acknowledge the facilities provided through the Central Instrument Facility (CIF) of Pondicherry University and DST-FIST and UGC-SAP Programmes coordinated by Prof. N. Sakthivel.

References

[1] S. Hamed-Akbari Tousi, M.R. Saberi, J. Chamani, Comparing the interaction of cyclophosphamide monohydrate to human serum albumin as opposed to holo-transferrin by spectroscopic and molecular modeling methods: evidence for allocating the binding site, Protein Pept. Lett. 17 (2010) 1524–1535, https://doi.org/10.2174/092986611009011524.

[2] F. Yang, Y. Zhang, H. Liang, Interactive association of drugs binding to human serum albumin, Int. J. Mol. Sci. 15 (2014) 3580–3595, https://doi.org/10.3390/ijms15033580.

[3] T.R.C. Guizado, Analysis of the structure and dynamics of human serum albumin, J. Mol. Model. 20 (2014) 2450, https://doi.org/10.1007/s00894-014-2450-y.

[4] S. Sugio, A. Kashima, S. Mochizuki, M. Noda, K. Kobayashi, Crystal structure of human serum albumin at 2.5 Å resolution, Protein Eng. 12 (1999) 439–446.

[5] B. Bakaeean, M. Kabiri, H. Iranfar, M.R. Saberi, J. Chamani, Binding effect of common ions to human serum albumin in the presence of norfloxacin: Investigation with spectroscopic and zeta potential approaches, J. Solution Chem. 41 (2012) 1777–1801, https://doi.org/10.1007/s10953-012-9895-3.

[6] K. Marita, K. Sand, M. Bern, J. Nilsen, H.T. Noordzij, I. Sandlie, J.T. Andersen, Unraveling the interaction between FcRn and albumin: opportunities for design of albumin-based therapeutics, Front. Immunol. 5 (2015) 1–21, https://doi.org/10.3389/fimmu.2014.00682.

[7] O.K. Abou-zied, Understanding the physical and chemical nature of the warfarin drug binding site in human serum albumin: experimental and theoretical studies, Curr. Pharm. Des. 21 (2015) 1800–1816, https://doi.org/10.2174/1381612821666150304163447.

[8] M.A. Cheema, P. Taboada, S. Barbosa, J. Juárez, M. Gutiérrez-Pichel, M. Siddiq, V. Mosquera, Human serum albumin unfolding pathway upon drug binding: A thermodynamic and spectroscopic description, J. Chem. Thermodyn. 41 (2009) 439–447, https://doi.org/10.1016/j.jct.2008.11.011.

[9] T. Chatterjee, A. Pal, S. Dey, B.K. Chatterjee, P. Chakrabarti, Interaction of virstatin with human serum albumin: Spectroscopic analysis and molecular modeling, PLoS One 7 (2012) 1–12, https://doi.org/10.1371/journal.pone.0037468.

[10] H.F. Jeremias, D. Lousa, A. Hollmann, A.C. Coelho, C.S. Baltazar, J.D. Seixas, A.R. Marques, N.C. Santos, C.C. Romão, C.M. Soares, Study of the interactions of bovine serum albumin with a molybdenum(II) carbonyl complex by spectroscopic and molecular simulation methods, PloS one 13 (2018) 1–15, https://doi.org/10.1371/journal.pone.0204624.g001.

[11] J.D. Seixas, A. Mukhopadhyay, T. Santos-Silva, L.E. Otterbein, D.J. Gallo, S.S. Rodrigues, B.H. Guerreiro, A.M. Goncalves, N. Penacho, A.R. Marques, A.C. Coelho, P.M. Reis, M.J. Romao, C.C. Romao, Characterization of a versatile organometallic pro-drug (CORM) for experimental CO based therapeutics, Dalt. Trans. 42 (2013) 5985–5998, https://doi.org/10.1039/c2dt32174b.

[12] M. Popova, T. Soboleva, A.M. Arif, L.M. Berreau, Properties of a flavonol-based photoCORM in aqueous buffered solutions: influence of metal ions, surfactants and proteins on visible light- induced CO release, RSC Adv 32 (2017) 21997–22007, https://doi.org/10.1039/c7ra02653f.

[13] Y. Zhang, Z. Zhang, Y. Gou, M. Jiang, H. Khan, Z. Zhou, H. Liang, F. Yang, Design an anticancer copper(II) pro-drug based on the flexible IIA subdomain of human serum albumin, J. Inorg. Biochem. 172 (2017) 1–8, https://doi.org/10.1016/j.jinorgbio.2017.04.002.

[14] V. Pichler, J. Mayr, P. Heffeter, O. Dömötör, É.A. Enyedy, G. Hermann, D. Groza, G. Köllensperger, M. Galanksi, W. Berger, B.K. Keppler, C.R. Kowol, Maleimide-functionalised platinum(IV) complexes as a synthetic platform for targeted drug delivery, Chem. Commun. 49 (2013) 2249–2251, https://doi.org/10.1039/c3cc39258a.

[15] P. Vidhyapriya, D. Divya, B. Manimaran, N. Sakthivel, Photoactivated $[Mn(CO)_3Br(\mu\text{-bpcpd})]_2$ induces apoptosis in cancer cells via intrinsic pathway, J. Photochem. Photobiol. B Biol. 188 (2018) 28–41, https://doi.org/10.1016/j.jphotobiol.2018.08.021.

[16] J. Li, J. Li, Y. Jiao, C. Dong, Spectroscopic analysis and molecular modeling on the interaction of jatrorrhizine with human serum albumin (HSA), Spectrochim Acta Part A Mol. Biomol. Spectrosc. 118 (2014) 48–54, https://doi.org/10.1016/j.saa.2013.07.029.

[17] T. Sohrabi, M. Hosseinzadeh, S. Beigoli, M.R. Saberi, J. Chamani, Probing the binding of lomefloxacin to a calf thymus DNA-histone H1 complex by multi-spectroscopic and molecular modeling techniques, J. Mol. Liq. 256 (2018) 127–138, https://doi.org/10.1016/j.molliq.2018.02.031.

[18] C. Ashok Kumar, D. Divya, R. Nagarajaprakash, V. Veena, P. Vidhyapriya, N. Sakthivel, B. Manimaran, Self-assembly of manganese(I) and rhenium(I) based semi-rigid ester functionalized M_2L_2-type metallacyclophanes: Synthesis, characterization and cytotoxicity evaluation, J. Organomet. Chem. 846 (2017) 152–160, https://doi.org/10.1016/j.jorganchem.2017.06.003.

[19] Z.Y. Tian, L.N. Song, Y. Zhao, F.L. Zang, Z.H. Zhao, N.H. Chen, X.J. Xu, C.J. Wang, Spectroscopic study on the interaction between naphthalimide-polyamine conjugates and bovine serum albumin (BSA), Molecules (2015), https://doi.org/10.3390/molecules200916491.

[20] L. Sułkowski, B. Pawełczak, M. Chudzik, M. Maciążek-Jurczyk, Characteristics of the protoporphyrin IX binding sites on human serum albumin using molecular docking, Molecules 21 (2016) 1519, https://doi.org/10.3390/molecules21111519.

[21] Z. Sharif-Barfeh, S. Beigoli, S. Marouzi, A.S. Rad, A. Asoodeh, J. Chamani, Multi-spectroscopic and HPLC studies of the interaction between estradiol and cyclophosphamide with human serum albumin: binary and ternary systems, J. Solution Chem. 46 (2017) 488–504, https://doi.org/10.1007/s10953-017-0590-2.

[22] X. Peng, X. Wang, W. Qi, R. Su, Z. He, Affinity of rosmarinic acid to human serum albumin and its effect on protein conformation stability, Food Chem. 192 (2016) 178–187, https://doi.org/10.1016/j.foodchem.2015.06.109.

[23] K. Żamojć, D. Jacewicz, L. Chmurzyński, Quenching of fluorescence of polycyclic aromatic hydrocarbons by 4-OH-TEMPO, Anal. Lett. 46 (2013) 349–355, https://doi.org/10.1080/00032719.2012.718830.

[24] T. Topală, A. Bodoki, L. Oprean, R. Oprean, Bovine serum albumin interactions with metal complexes, Clujul Med. 87 (2014) 215–219, https://doi.org/10.15386/cjmed-357.

[25] X. Ma, J. Yan, K. Xu, L. Guo, H. Li, Binding mechanism of trans -N-caffeoyltyramine and human serum albumin: Investigation by multi-spectroscopy and docking simulation, Bioorg. Chem. 66 (2016) 102–110, https://doi.org/10.1016/j.bioorg.2016.04.002.

[26] S. Ranjbar, Y. Shokoohinia, S. Ghobadi, N. Bijari, S. Gholamzadeh, N. Moradi, M.R. Ashrafi-kooshk, A. Aghaei, R. Khodarahmi, Studies of the interaction between isoimperatorin and human serum albumin by multispectroscopic method: identification of possible binding site of the compound using esterase activity of the protein, Sci. World J. (2013), https://doi.org/10.1155/2013/305081.

[27] A. Varlan, M. Hillebrand, Bovine and human serum albumin interactions with 3-carboxyphenoxathiin studied by fluorescence and circular dichroism spectroscopy, Molecules 15 (2010) 3905–3919, https://doi.org/10.3390/molecules15063905.

[28] S. Rashidipour, S. Naeeminejad, J. Chamani, Study of the interaction between DNP and DIDS with human hemoglobin as binary and ternary systems: spectroscopic and molecular modeling investigation, J. Biomol. Struct. Dyn. 34 (2016) 57–77, https://doi.org/10.1080/07391102.2015.1009946.

[29] J. Thipperudrappa, D.S. Biradar, M.T. Lagare, S.M. Hanagodimath, S.R. Inamdar, J.S. Kadadevaramath, Fluorescence quenching of BPBD by aniline in benzene-acetonitrile mixtures, J. Photochem. Photobiol. A Chem. 177 (2006) 89–93, https://doi.org/10.1016/j.jphotochem.2005.05.016.

[30] B. Chakraborty, S. Basu, Interaction of BSA with proflavin: a spectroscopic approach, J. Lumin. 129 (2009) 34–39, https://doi.org/10.1016/j.jlumin.2008.07.012.

[31] P. Lakshmi, M. Mondal, K. Ramadas, S. Natarajan, Molecular interaction of 2,4-diacetylphloroglucinol (DAPG) with human serum albumin (HSA): The spectroscopic, calorimetric and computational investigation, Spectrochim. Acta Part A Mol. Biomol. Spectrosc. 183 (2017) 90–102, https://doi.org/10.1016/j.saa.2017.04.012.

[32] Y.Y. Wang, M. Zhu, F. Liu, X. Wu, D. Pan, J. Liu, S. Fan, Z. Wang, J. Tang, R. Na, Q.X. Li, R. Hua, S. Liu, Comparative studies of interactions between fluorodihydroquinazolin derivatives and human serum albumin with fluorescence spectroscopy, Molecules 21 (2016) 1373, https://doi.org/10.3390/molecules21101373.

[33] J. Min, X. Meng-Xia, Z. Dong, L. Yuan, L. Xiao-Yu, C. Xing, Spectroscopic studies on the interaction of cinnamic acid and its hydroxyl derivatives with human serum albumin, J. Mol. Struct. 692 (2004) 71–80, https://doi.org/10.1016/j.molstruc.2004.01.003.

[34] H. Xu, N. Yao, H. Xu, T. Wang, G. Li, Z. Li, Characterization of the interaction between eupatorin and bovine serum albumin by spectroscopic and molecular modeling methods, Int. J. Mol. Sci. 14 (2013) 14185–14203, https://doi.org/10.3390/ijms140714185.

[35] J. Chamani, M. Heshmati, Mechanism for stabilization of the molten globule state of papain by sodium n-alkyl sulfates: Spectroscopic and calorimetric approaches, J. Coll. Interf. Sci. 322 (2008) 119–127, https://doi.org/10.1016/j.jcis.2008.03.001.

[36] S. Roy, S. Ganai, R.K. Nandi, K.C. Majundar, T.K. Das, Studies of the interaction of bovine serum albumin with pyrimidine-annulated spirodihydrofuran and its biological activities, Adv. Mater. Lett. 6 (2015) 1018–1024, https://doi.org/10.5185/amlett.2015.5933.

[37] J. Chamani, N. Tafrishi, M. Momen-Heravi, Characterization of the interaction between human lactoferrin and lomefloxacin at physiological condition: Multi-spectroscopic and modeling description, J. Lumin. 130 (2010) 1160–1168, https://doi.org/10.1016/j.jlumin.2010.02.014.

[38] C. Li, T. Huang, Y. Fu, Y. Liu, S. Zhou, Z. Qi, C. Li, Interaction of di-2-pyridylketone 2-pyridine carboxylic acid hydrazone and its copper complex with BSA: effect on antitumor activity as revealed by spectroscopic studies, Molecules 21 (2016) 21050563, https://doi.org/10.3390/molecules21050563.

[39] D. Bose, D. Sarkar, N. Chattopadhyay, Probing the binding interaction of a phenazinium dye with serum transport proteins: A combined fluorometric and circular dichroism study, Photochem. Photobiol. 86 (2010) 538–544, https://doi.org/10.1111/j.1751-1097.2009.00688.x.

[40] M. Kabiri, Z. Amiri-tehranizadeh, A. Baratian, M.R. Saberi, J. Chamani, Use of spectroscopic, zeta potential and molecular dynamic techniques to study the

interaction between human holo-transferrin and two antagonist drugs: comparison of binary and ternary systems, Molecules (2012), https://doi.org/10.3390/molecules17033114.
[41] N. Sreerama, R.W. Woody, Estimation of protein secondary structure from circular dichroism spectra: comparison of CONTIN, SELCON, and CDSSTR methods with an expanded reference set, Anal. Biochem. 287 (2000) 252–260, https://doi.org/10.1006/abio.2000.4880.
[42] J. Chamani, Comparison of the conformational stability of the non-native α-helical intermediate of thiol-modified β-lactoglobulin upon interaction with sodium n-alkyl sulfates at two different pH, J. Coll. Interf. Sci. 299 (2006) 636–646, https://doi.org/10.1016/j.jcis.2006.02.049.
[43] V.D. Suryawanshi, L.S. Walekar, A.H. Gore, P.V. Anbhule, G.B. Kolekar, Spectroscopic analysis on the binding interaction of biologically active pyrimidine derivative with bovine serum albumin, J. Pharm. Anal. 6 (2016) 56–63, https://doi.org/10.1016/j.jpha.2015.07.001.
[44] B. Mishra, A. Barik, K.I. Priyadarsini, H. Mohan, Fluorescence spectroscopic studies on binding of a flavonoid antioxidant quercetin to serum albumins, J. Chem. Sci. 117 (2005) 641–647, https://doi.org/10.1007/BF02708293.
[45] Y. Shi, H. Liu, M. Xu, Z. Li, G. Xie, L. Huang, Z. Zeng, Spectroscopic studies on the interaction between an anticancer drug ampelopsin and bovine serum albumin, Spectrochim Acta Part A Mol. Biomol. Spectrosc. 87 (2012) 251–257, https://doi.org/10.1016/j.saa.2011.11.048.
[46] A. Bouhekka, T. Bürgi, In situ ATR-IR spectroscopy study of adsorbed protein: Visible light denaturation of bovine serum albumin on TiO_2, Appl. Surf. Sci. 261 (2012) 369–374, https://doi.org/10.1016/j.apsusc.2012.08.017.
[47] F. Manouchehri, Y. Izadmanesh, E. Aghaee, J.B. Ghasemi, Experimental, computational and chemometrics studies of BSA-vitamin B6 interaction by UV – Vis, FT-IR, fluorescence spectroscopy, molecular dynamics simulation and hard-soft modeling methods, Bioorg. Chem. 68 (2016) 124–136, https://doi.org/10.1016/j.bioorg.2016.07.014.
[48] R.I. Litvinov, D.A. Faizullin, Y.F. Zuev, J.W. Weisel, The α-helix to β-sheet transition in stretched and compressed hydrated fibrin clots, Biophys. J. 103 (2012) 1020–1027, https://doi.org/10.1016/j.bpj.2012.07.046.